Phase diagram of a generalized t-J model: Renormalization-group approach

Sergio A. Cannas*
Facultad de Matemática, Astronomía y Física, Universidad Nacional de Córdoba, Laprida 854, 5000 Córdoba, Argentina

Constantino Tsallis
Centro Brasileiro de Pesquisas Físicas, Conselho Nacional de Desenvolvimento Científico e Tecnológico, Rua Xavier Sigaud 150, 22290 Rio de Janeiro, Rio de Janeiro, Brazil

(Received 15 October 1991)

A generalized t-J Hamiltonian is analyzed within the framework of a quantum real-space renormalization group. Besides the usual hopping (t), exchange (J), and chemical-potential (μ) terms, the Hamiltonian contains a nearest-neighbor charge interaction term and is invariant under the renormalization. The finite-temperature phase diagram of the $d=2$ and $d=3$ model is calculated in the full range of the parameters. Our results show that many of the critical properties of the La- and Y-based high-T_c superconductors can be explained by the present model.

I. INTRODUCTION

The t-J model has received intensive attention in recent years since Anderson[1] suggested that it contains the relevant physics of the high-T_c materials, at least those containing copper-oxide planes. The model is described by a lattice Hamiltonian of hard-core fermions and includes hopping (t) and antiferromagnetic exchange interactions (J). This Hamiltonian is related to the strong-coupling limit of the Hubbard Hamiltonian ($U/t \gg 1$ in the standard notation) by a canonical transformation[2] within which appears the correspondence $J/t = t/2U \ll 1$. On the other hand, Zhang and Rice[3] derived with some approximations the t-J model directly from a CuO multiband Hamiltonian, finding values of J/t somewhat larger tan $t/2U$; consequently, the entire range of J/t (and not only $J/t \ll 1$) must be studied. Since the experimental evidence strongly supports the assumption that high-T_c superconductivity is an effect mainly due to the doped CuO_2 layers of the ceramic compounds, most of the work has focused the *two*-dimensional t-J model. However, neutron-diffraction experiments[4,5] have shown a three-dimensional long-range antiferromagnetic order in both La and Y compounds with a rather high Néel temperature; the long-range order is probably originated by weak-interplane exchange couplings. Therefore, it is also interesting to investigate the magnetic properties of the finite-temperature phase diagram for the *three*-dimensional t-J model.

Since there are no exact solutions for the t-J model in dimensions $d > 1$ (and only a few ones for $d = 1$, see, for instance, Ref. 6) many approaches (e.g., Lanczos method,[7] and approximations based on finite clusters[8] have been applied to the study of several of its properties. However, most of the effort has been devoted to the zero-temperature properties of this model. Using a quantum real-space renormalization-group (RG) scheme, we analyze in this paper the finite-temperature phase diagram of a convenient generalization of the t-J model. Such a model is described by a Hamiltonian which contains, besides the hopping and exchange terms, a nearest-neighbor charge interaction (K) as well as the chemical potential term (μ). This model is invariant in form under RG and can be obtained as the $U \to \infty$ limit of an even more general Hubbard Hamiltonian,[9] which also remains invariant under RG.

Our RG procedure is based on a calculation performed for a two-terminal cluster whose iterations yield an hierarchical lattice. Let us anticipate that the results are not exact for the hierarchical lattice because of the noncommutativity of the involved operators. However, the results are asymptotically exact at high temperature and believed to be a good approximation for a wide range of temperatures. To the best of our knowledge this is the first calculation of the full phase diagram at finite temperature for the present model.

In Sec. II, we derive the generalized t-J Hamiltonian and some of its basic properties are briefly reviewed. In Sec. III, we discuss the RG formalism and we analyze the RG recurrence equations for some particular cases. A numerical calculation of the $d=2$ phase diagram is presented in Sec. IV; the existence of first-order phase transitions (two-phase coexistence)[10] is analyzed for different values of J/t. In Sec. V, we analyze the $d=3$ phase diagram, which turns out to be very rich one. Our results suggest that the $d=3$ generalized t-J model could, at least qualitatively, describe the phenomenology of the magnetic phase diagram of some copper-oxide superconductors. We finally conclude in Sec. VI.

II. THE MODEL

Let us consider a system of hard-core fermions on a lattice, i.e., we assume that each lattice site can be occupied by, at most, one particle. Then the dimensionless t-J model is defined by the following Hamiltonian:

$$\mathcal{H}_{t\text{-}J} \equiv -\beta H_{t\text{-}J} = t \sum_{\langle i,j\rangle,\sigma} (a^{\dagger}_{i,\sigma} a_{j,\sigma} + a^{\dagger}_{j,\sigma} a_{i,\sigma}) - J \sum_{\langle i,j\rangle} \mathbf{S}_i \cdot \mathbf{S}_j + \mu \sum_{i,\sigma} n_{i,\sigma} , \quad (1)$$

where $\beta \equiv 1/k_B T$, $a^{\dagger}_{i,\sigma} \equiv (1-n_{i,-\sigma}) c^{\dagger}_{i,\sigma}$, $c^{\dagger}_{i,\sigma}$ creates an electron with spin $\sigma = \uparrow, \downarrow$ in a Wannier state centered at the site i of the lattice, $n_{i,\sigma} \equiv c^{\dagger}_{i,\sigma} c_{i,\sigma}$; t, J, and μ are, respectively, the dimensionless hopping constant, exchange interaction ($J > 0$ corresponds to antiferromagnetic coupling), and chemical potential; $\langle i,j \rangle$ runs over all pairs of first-neighboring sites on a d-dimensional hypercubic lattice. The $a^{\dagger}_{i,\sigma}$ operators are introduced in order to properly take into account the constraint of no-double occupancy. The spin operators $\mathbf{S}_i$ are defined by

$$\mathbf{S}_i \equiv \sum_{\alpha,\beta} c^{\dagger}_{i,\alpha} \boldsymbol{\sigma}_{\alpha,\beta} c_{i,\beta} , \quad (2)$$

where $\boldsymbol{\sigma}$ are the Pauli matrices and $\alpha, \beta = \uparrow, \downarrow$.

There is another version of the t-J Hamiltonian that sometimes appears in the literature, namely,

$$\mathcal{H}_{t\text{-}J} = t \sum_{\langle i,j\rangle\sigma} (a^{\dagger}_{i,\sigma} a_{j,\sigma} + a^{\dagger}_{j,\sigma} a_{i,\sigma}) - J \sum_{\langle i,j\rangle} (\mathbf{S}_i \cdot \mathbf{S}_j - n_i n_j) + \mu \sum_{i,\sigma} n_{i,\sigma} , \quad (3)$$

where $n_i \equiv n_{i,\uparrow} + n_{i,\downarrow}$. This Hamiltonian is derived approximately in the strong-coupling limit $U \gg t$ of the Hubbard model by a canonical transformation.[2,12] Such procedure yields, for the Hamiltonian (3), the value $J = t^2/2U$.[13] In order to avoid confusion, let us stress that the Hamiltonian (3) is, in general, different from the Hamiltonian (1) (they only coincide if the total number of electrons precisely coincides with the number of sites); very unfortunately they are *both* commonly referred to as the t-J model. The generalized Hamiltonian we shall introduce here contains both as particular cases.

In order to study the critical properties of the t-J model at finite temperature, we use a real-space renormalization-group method. The procedure consists of replacing d-dimensional hypercubic Bravais lattices by d-dimensional diamond like hierarchical lattices. Such lattices are defined through infinite iterations on a two-terminal cluster, which consists in an array of l^{d-1} strings in parallel, each string being constituted by l bonds in series. Some typical clusters are shown in Fig. 1 ($l = 3$). The RG recurrence equations are then obtained by explicitly computing the partial trace

$$\exp(\mathcal{H}' + \mathcal{C}) = \operatorname*{Tr}_{\text{internal sites}} \exp(\mathcal{H}) , \quad (4)$$

where $\mathcal{H}$ denotes the Hamiltonian of the cluster and $\mathcal{H}'$ denotes the Hamiltonian of the renormalized two-site cluster (see Fig. 1). The partial trace is calculated by summing the matrix elements of $\exp(\mathcal{H})$ over the set of occupation numbers $\{n_{i,\sigma}\}$ associated with the *internal* sites of the cluster. Such a procedure neglects, at every iteration, the noncommutativity between the Hamiltonians associated with first-neighboring clusters. This approximation is asymptotically exact at high temperatures (see Ref. 14 and references therein). Neither the Hamiltonian (1) nor the Hamiltonian (3) satisfy relation (4); in other words, if $\mathcal{H}$ is a t-J Hamiltonian, the resulting $\mathcal{H}'$ may contain new terms that were not present in $\mathcal{H}$. In a previous work,[9] we derived a generalized Hubbard Hamiltonian whose form is preserved by the RG transformation (4), namely,

$$\begin{aligned}\mathcal{H}^{\mu}_{G} = {} & t \sum_{\langle i,j\rangle,\sigma} (c^{\dagger}_{i,\sigma} c_{j,\sigma} + c^{\dagger}_{j,\sigma} c_{i,\sigma}) + U \sum_{i} n_{i,\uparrow} n_{i,\downarrow} + \mu \sum_{i,\sigma} n_{i,\sigma} - J \sum_{\langle i,j\rangle} \mathbf{S}_i \cdot \mathbf{S}_j - K \sum_{\langle i,j\rangle} (S^z_i)^2 (S^z_j)^2 \\ & + Y \sum_{\langle i,j\rangle} \boldsymbol{\rho}_i \cdot \boldsymbol{\rho}_j - I \sum_{\langle i,j\rangle} [\rho^z_i \rho^z_j - (\rho^x_i \rho^x_j + \rho^y_i \rho^z_j)] + R \sum_{\langle i,j\rangle} [(\rho^z_i)^2 \rho^z_j + (\rho^z_j)^2 \rho^z_i] \\ & + D \sum_{\langle i,j\rangle,\sigma} (c^{\dagger}_{i,\sigma} c_{j,\sigma} + c^{\dagger}_{j,\sigma} c_{i,\sigma})(n_{i,-\sigma} - n_{j,-\sigma})^2 + E \sum_{\langle i,j\rangle,\sigma} (c^{\dagger}_{i,\sigma} c_{j,\sigma} + c^{\dagger}_{j,\sigma} c_{i,\sigma}) n_{i,-\sigma} n_{j,-\sigma} , \end{aligned} \quad (5)$$

where the charge operators are defined by

$$\begin{aligned} \rho^z_i &\equiv n_{i,\uparrow} + n_{i,\downarrow} - 1 , \\ \rho^+_i &\equiv c^{\dagger}_{i,\sigma} c^{\dagger}_{i,\downarrow} , \\ \rho^-_i &\equiv c_{i,\downarrow} c_{i,\uparrow} , \end{aligned} \quad (6)$$

$$\begin{aligned} \rho^x_i &\equiv \rho^+_i + \rho^-_i , \\ \rho^y_i &\equiv -i(\rho^+_i - \rho^-_i) . \end{aligned} \quad (7)$$

The Hamiltonian (5) is the minimal one that contains the Hubbard Hamiltonian as a particular case and remains invariant under the RG transformation. In order to obtain a generalization of Hamiltonians (1) and (3) that satisfy relation (4), we should first impose the constraint of no-double occupancy to the Hamiltonian $\mathcal{H}^{\mu}_{G}$. Such a constraint can be achieved by taking the limit $U \to +\infty$ in Eq. (5) while keeping finite all the other parameters. In this limit the states with doubly occupied sites will not contribute at all and the effective resulting Hamiltonian will have nonzero matrix elements only between states belonging to the subspace of no-double occupancy, i.e., those states which satisfy $n_{i,\uparrow} n_{i,\downarrow} = 0$ for all sites i. In this case the only remaining hopping processes will be those that only connect sites with single or null occupancy; such a condition can be made explicit by setting $D = E = -t$. Since the non diagonal charge operators ρ^x_i, ρ^y_i only connect states having null and double occupancy, the corresponding terms in Eq. (5) will not contribute at all. Furthermore, since $n_{i,\uparrow} n_{i,\downarrow} = 0$ for all sites

i, we find that

$$(\rho_i^z)^2=-\rho_i^z=1-(S_i^z)^2 , \tag{8}$$

$$(S_i^z)^2=n_i . \tag{9}$$

From Eqs. (8) and (9) we see that the terms in Eq. (5) containing the diagonal charge operators ρ_i^z can be absorbed in the terms associated with the K and μ parameters. Therefore, the resulting Hamiltonian can be written as follows:

$$\mathcal{H}_S=t\sum_{\langle i,j\rangle,\sigma}(a_{i,\sigma}^{\dagger}a_{j,\sigma}+a_{j,\sigma}^{\dagger}a_{i,\sigma})-J\sum_{\langle i,j\rangle}\mathbf{S}_i\cdot\mathbf{S}_j -K\sum_{\langle i,j\rangle}(S_i^z)^2(S_j^z)^2+\mu\sum_{i,\sigma}n_{i,\sigma} . \tag{10}$$

The term associated with the parameter K in the Hamiltonian (10) can be rewritten [by using Eq. (9)] as $\sum_{\langle i,j\rangle}n_in_j$ so it describes a nearest-neighbor charge interaction. Setting $K=0$ in Eq. (10), we recover the Hamiltonian (1), while for $K=-J$ we recover the Hamiltonian (3). The subindex S in the Hamiltonian (10) makes reference to Schlottmann who first proposed[11] this Hamiltonian in the context of heavy-fermion systems ($K\equiv V$ in Schlottmann's notation).

The Hamiltonian $\mathcal{H}_G^{\mu}$ was derived by constructing the most general Hamiltonian which satisfies some basic symmetries of the Hubbard Hamiltonian to be preserved through the partial trace (4). It can be seen that all these symmetry properties are still preserved in the $U\rightarrow\infty$ limit procedure used to derive the Hamiltonian (10) from the Hamiltonian (5). Therefore, the Hamiltonian (10) is the simplest one that contains the t-J model (in both of its versions) as a particular case and remains invariant under the RG transformation. All the above-mentioned symmetry arguments, as well as the problem of the correct choice of the cluster in this procedure, are discussed in detail in Ref. 14. By using the same arguments, it can be shown that, in the presence of an external magnetic field, the Hamiltonian which remains invariant under RG is $\mathcal{H}_S+\mathcal{H}_B$,[14] with

$$\mathcal{H}_B=B\sum_i S_i^z-J_2\sum_{\langle i,j\rangle}[S_i^zS_j^z-(S_i^xS_j^x+S_i^yS_j^y)] +R_2\sum_{\langle i,j\rangle}[(S_i^z)^2S_j^2+(S_j^z)^2S_i^z] . \tag{11}$$

Let us mention some important properties of the Hamiltonian (10). First, we can easily verify that

$$[\mathcal{H}_S,\mathbf{S}]=\mathbf{0} , \tag{12}$$

$$[\mathcal{H}_S,N]=0 , \tag{13}$$

where $\mathbf{S}\equiv\sum_i\mathbf{S}_i$ and $N\equiv\sum_i n_i$, respectively, are the total spin and total number of particles operators. By means of a unitary transformation,[15] it can be seen that the spectrum of $\mathcal{H}_S$ is invariant under the change of sign of the parameter t. Hence, the grand-partition function

$$Z=\mathrm{Tr}\exp(\mathcal{H}_S) \tag{14}$$

satisfies $Z(t)=Z(-t)$ and the phase diagram which results is symmetric under the transformation $t\rightarrow -t$. For definiteness we assume $t>0$.

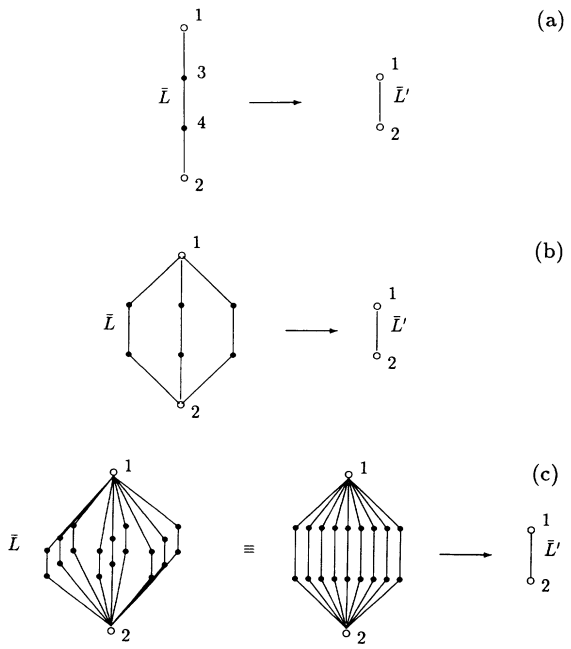

FIG. 1. Renormalization-group cell transformation. Every two-rooted cluster generates, through infinite iterations, a hierarchial lattice of intrinsic dimmensionality d. $\bar{L}$ stands for the set of parameters of the Hamiltonian; ○ and ● denote internal and terminal sites, repectively. (a) $d=2$; (b) $d=3$.

III. THE RENORMALIZATION GROUP

A. General considerations

The RG procedure is carried out in two steps. First we perform an exact calculation of the partial trace (4) for a linear four-site cluster [see Fig. 1(a)], by summing the matrix elements of $\exp(\mathcal{H}_S)$ over the set of occupation numbers $\{n_{3,\sigma},n_{4,\sigma}\}$. This calculation yields the recurrence equations between the set of parameters $\bar{L}\equiv(\mu,K,J,t)$ of the Hamiltonian $\mathcal{H}_S$ associated with the four-site chain and the set of renormalized parameters $\bar{L}'\equiv(\mu',K',J',t')$ of the Hamiltonian $\mathcal{H}_S'$ (associated with the two-site cluster); therefore we obtain

$$\bar{L}'=\bar{L}'_1(\bar{L}) , \tag{15}$$

where the subindex 1 stands for $d=1$. In the second step we consider a more general diamondlike cluster of the type shown in Figs. 1(a)–1(c). Every cluster of this kind consists in a parallel array of l^{d-1} four-site chains, where d is the intrinsic dimensionality of the hierarchical lattice and $l=3$ is the length scale of the RG transformation. The Hamiltonian associated with each of these clusters can be expressed as a sum of linear-chain Hamiltonians. Therefore, neglecting the noncommutativity between the linear-chain Hamiltonians,[14] the following approximate recurrence relations are obtained:

$$\bar{L}'=\bar{L}'_d(\bar{L})=l^{d-1}\bar{L}'_1(\bar{L}) . \tag{16}$$

These equations determine the flow of points in the (μ,K,J,t) parameters space for $d=2$ and 3 and enable

the calculation of the corresponding phase diagram as well as various critical exponents.

The calculation of Eq. (15) involves the exact diagonalization of $\mathcal{H}_S$. The subspace with no double occupancy of the Fock space $|\{n_{i,\sigma}\}\rangle$ associated with the four-site chain is a 3^4-dimensional one; in such a subspace $\mathcal{H}_S$ is represented by an 81×81 matrix. By using the fact that the basis vectors are simultaneously eigenvectors of N and S^z [see Eqs. (12) and (13)], we can present $\mathcal{H}_S$ in a block-diagonal structure by simply rearranging the order of these vectors according to the eigenvalues of N and $\mathbf{S}^z$. Even so, the largest irreducible blocks are, in general, analytically untractable and part of the calculation must be done numerically. We found that all the relevant fixed points of the recurrence equation (16) are located at the $t=0$ subspace of the (μ,K,J,t) space. In fact, for this particular case the recurrence equations can be derived analytically. In Secs. IV and IV, we derive the phase diagram generated by the general recurrence equation (16) for $d=2$ and 3, respectively; nevertheless, it is convenient to discuss now some general properties of the $t=0$ recurrence equations.

B. The $t=0$ recurrence equations

For $t=0$, the Hamiltonian (10) takes the form

$$\mathcal{H}=-J\sum_{\langle i,j\rangle}\mathbf{S}_i\cdot\mathbf{S}_j-K\sum_{\langle i,j\rangle}(S_i^z)^2(S_j^z)^2+\mu\sum_i(S_i^z)^2\ , \tag{17}$$

where we have used Eq. (9). Although this Hamiltonian looks like a quantum-mechanical analog of the BEG (Blume-Emery-Griffiths) Hamiltonian,[16,17] the situation is actually more complex. This is due to the fact that the $\mathbf{S}_i$ operators cannot be interpreted as standard spin-1 operators. Since the condition $t=0$ is preserved through Eq. (16), the subspace $(\mu,K,J,0)$ constitutes an invariant one under RG. In this case we obtain

$$\begin{aligned}
\mu' &= 2l^{d-1}\ln\left[\frac{F_2}{F_1}\right]\ ,\\
K' &= -J'+l^{d-1}\ln\left[\frac{F_2^2}{F_1F_3}\right]\ ,\\
J' &= \frac{l^{d-1}}{2}\operatorname{arctanh}\left[-\frac{F_5}{F_4}\right]\ ,
\end{aligned} \tag{18}$$

where

$$\begin{aligned}
F_1 &\equiv 1+4\exp(\mu)+2\exp(2\mu-K)g_5(J)\ ,\\
F_2 &\equiv \exp(\mu/2)[1+2\exp(\mu)+\exp(2\mu-2K)g_4(J)\\
&\quad +\exp(\mu-K)g_5(J)],\\
F_3 &\equiv \exp(\mu)+2\exp(2\mu-K)g_5(J)\\
&\quad +\exp(3\mu-3K)g_1(J)\ ,\\
F_4 &\equiv \exp(\mu)+2\exp(2\mu-K)g_5(J)\\
&\quad +\exp(3\mu-3K)g_2(J)\ ,\\
F_5 &\equiv \exp(3\mu-3K)g_3(J)\ ,
\end{aligned} \tag{19}$$

with

$$\begin{aligned}
g_1(x) &\equiv \exp(x)+\tfrac{5}{3}\exp(-3x)+\tfrac{1}{3}\exp(3x)\cosh(2\sqrt{3}x)\\
&\quad +\exp(x)\left[\cosh(2\sqrt{2}x)+\frac{1}{\sqrt{2}}\sinh(2\sqrt{2}x)\right]\ ,\\
g_2(x) &\equiv \tfrac{1}{2}\exp(x)+\tfrac{5}{6}\exp(-3x)+\tfrac{2}{3}\exp(3x)\cosh(2\sqrt{3}x)\\
&\quad +\exp(x)\left[2\cosh(2\sqrt{2}x)-\frac{1}{\sqrt{2}}\sinh(2\sqrt{2}x)\right]\ ,\\
g_3(x) &\equiv g_1(x)-g_2(x)\ ,\\
g_4(x) &\equiv 1+2\exp(-2x)+\exp(4x)\ ,\\
g_5(x) &\equiv \exp(-x)+\exp(x)\cosh(2x)\ .
\end{aligned} \tag{20}$$

From Eqs. (18)–(20), we find that $J=0$ further constitutes an invariant subspace under RG (i.e., $J=0$ implies $J'=0$). Some general properties of the phase diagram in this subspace can be easily deduced by noting that, for $J=0$, the Hamiltonian (17) takes the form

$$\mathcal{H}=-K\sum_{\langle i,j\rangle}n_in_j+\mu\sum_i n_i\ . \tag{21}$$

Defining a new variable t_i at each site i as

$$t_i\equiv 2(n_i-\tfrac{1}{2})\quad (t_i=\pm 1)\ , \tag{22}$$

the Hamiltonian (21) can be mapped into a spin-$\frac{1}{2}$ Ising model with an effective (temperature-dependent) external field[18]

$$\mathcal{H}_I=-\tfrac{1}{4}K\sum_{\langle i,j\rangle}t_it_j+\sum_i B_it_i\ , \tag{23}$$

where

$$B_i\equiv\tfrac{1}{2}(\mu-\tfrac{1}{2}z_iK+\ln 2) \tag{24}$$

and z_i is the coordination number of the site i. For a Bravais lattice, $z_i=z$ is a constant and the resulting field B_i is homogeneous; for a hierarchical lattice, z_i is site dependent and then B_i is a local field. The line $K=0$ in the plane (μ,K) is also an invariant subspace of the RG (i.e., $K=0\Longrightarrow K'=0$). This subspace is associated with a noninteracting system which corresponds, in the magnetic analog [see Eq. (23)], to a free spin system in a magnetic field. Along this line we find three fixed points: (i) the semistable fixed point $(\mu,K,J,t)=(0,0,0,0)$, hereafter denoted by q; (ii) the fully stable fixed point $(+\infty,0,0,0)$, which we denote by p; and (iii) the fully stable fixed point $(-\infty,0,0,0)$, hereafter denoted by h. Through Eq. (24) we can see that the fixed point p is associated with a phase characterized by $\langle t_i\rangle>0$, which is equivalent [see Eq. (22)] to $\langle n_i\rangle>\frac{1}{2}$; consequently, this phase is an *electron-rich* (high density of electrons) one. The fixed point h is associated with a phase characterized by $\langle t_i\rangle<0$, which is equivalent [see Eq. (22)] to $\langle n_i\rangle<\frac{1}{2}$; therefore, it describes a *hole-rich* phase (low density of electrons). Both phases (electron rich and hole rich) are paramagnetic ones. For $K<0$, the Hamiltonian (23) describes a ferromagnetic model and a first-order transition line between the above two phases is expected for $d>1$.

For $K>0$, the Hamiltonian (23) describes an antiferromagnetic Ising model and, consequently, for $d>1$ an antiferromagneticlike ordered phase is expected in some region of the $K>0$ half of the (μ,K) plane. In other words, if we divide the lattice into two interpenetrating first-neighboring sublattices, $\langle t_i\rangle>0$ for all sites of one sublattice $\langle t_i\rangle<0$ for the other one. Through Eq. (22) we can see that the sites of one sublattice are predominantly in the state $n_i=0$, whereas the sites of the other one are inn the state $n_i=1$. This situation corresponds to a *charge-density-wave* (CDW) phase. The total density of electrons in this phase is $n\equiv\sum_i\langle n_i\rangle/\mathcal{N}=\frac{1}{2}$, where $\mathcal{N}$ is the number of lattice sites.

Let us now consider some important limits of the $J\neq 0$ case. From Eqs. (18)–(20), we find, in the limit $\mu\to+\infty$, the following asymptotic behaviors:

$$\begin{aligned}&\mu'\sim l^{d-1}\mu\ ,\\ &K'\sim f_2(d,J)\ ,\\ &J'\sim f_1(d,J)\ ,\end{aligned}\tag{25}$$

where

$$f_1(d,J)=\frac{l^{d-1}}{2}\operatorname{arctanh}\left[-\frac{g_3(J)}{g_2(J)}\right]\ ,\tag{26}$$

$$f_2(d,J)\equiv l^{d-1}\ln\left[\frac{g_4^2(J)}{2g_1(J)g_5(J)}\right]-f_1(d,J)\ .\tag{27}$$

We see that the recurrence equations (25) decouple and the only nontrivial one is that of the exchange coupling J. This fact can be easily understood if we notice that, in the limit $\mu\to+\infty$, the density of electrons $n\to 1$, i.e., all sites are occupied. In such situation the charge interaction term in the Hamiltonian (17) becomes just an irrelevant additive constant, the Hamiltonian thus becoming equivalent to the following one:

$$\mathcal{H}\sim -J\sum_{\langle i,j\rangle}\boldsymbol{\sigma}_i\cdot\boldsymbol{\sigma}_j\ ,\tag{28}$$

where $\boldsymbol{\sigma}_i$ are the Pauli matrices at the site i, i.e., we recover the isotropic spin-$\frac{1}{2}$ Heisenberg model. The function $f_1(d,J)$ is depicted in Fig. 2 for $d=2$ and 3, for both signs of J. The recurrence Eqs. (25) yield, for $d=2$, only trivial fixed points, i.e, there is [as expected from Eq. (28)] no phase transition into any magnetically ordered phase. The trivial fixed point $J=0$ corresponds to the already described fixed point $(\mu,K,J,t)=(+\infty,0,0,0)$. For $d=3$, $f_1(d,J)$ exhibits two nontrivial fixed points: an antiferromagnetic critical point $J_c^A\approx 0.353$ and a ferromagnetic one $J_c^F\approx -0.522$. Beside them there are two other stable fixed points, namely, an antiferromagnetic attractor $J_2^A\approx 2.457$ and a ferromagnetic one $J_2^F=-\infty$. Note that the antiferromagnetic attractor appears at a finite value instead of the usual $J=+\infty$ (zero-temperature) value. This shift of the zero-temperature fixed point is probably due to the high-temperature approximation made in the RG procedure. This behavior has already been encountered in other related works (see Ref. 14 and references therein). The fixed points of $f_1(3,J)$ provide, through Eqs. (25) and (27) the following set of fixed points for Eqs. (18): $(\mu,K,J)=(+\infty,K_c^A,J_c^A)$, $(+\infty,K_2^A,J_2^A)$, $(+\infty,K_c^F,J_c^F)$, $(+\infty,+\infty,-\infty)$, with $K_c^A\approx -0.001$, $K_2^A\approx -18.78$, and $K_c^F\approx 0.328$.

Another interesting asymptotic behavior occurs for $\mu\to-\infty$ and $K\to-\infty$. Let us first consider the case $J=0$. We first propose

$$K=\mu+\ln\alpha_0\ .\tag{29}$$

We then use Eqs. (18)–(20) and impose that, in the $\mu\to-\infty$ limit, $K'\sim\mu'+\ln\alpha_0$. We straightforwardly obtain

$$\mu'\sim l^{d-1}\mu\tag{30}$$

and

$$\ln\alpha_0=2\frac{l^{d-1}}{l^d-1}\ln 2\ .\tag{31}$$

In other words, the line determined by Eq. (29) is an

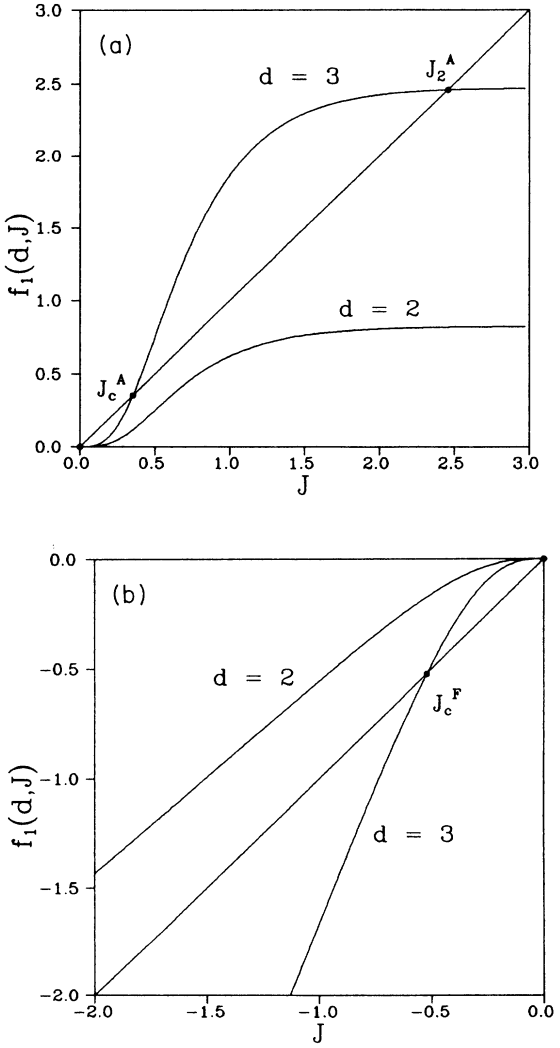

FIG. 2. Asymptotic recurrence relation $J'=f_1(d,J)$ corresponding to the Hamiltonian (17) in the limit $\mu\to\infty$ for dimensionalities $d=2$ and 3. (a) $J>0$; (b) $J<0$.

asymptotically invariant line under the RG for $J=0$. The existence of this line is numerically confirmed in Secs. IV and V. The point $(\mu,K,J)=(-\infty,-\infty,0)|_{K=\mu+\ln\alpha_0}$ is a fixed one of the RG equations. If we calculate the Jacobian of the recurrence Eqs. (18) for $J=0$ and we take the limit $\mu\to-\infty$ [with Eq. (29)], we find a relevant (greater than one) eigenvalue $\lambda=l^d$, whose associated eigenvector is $(\mu,K)=(1,0)$. The physical meaning of this fixed point will be discussed in Sec. IV.

Let us now consider the $J\neq0$ case. In the limit $\mu\to-\infty$ with $K=\mu+\text{const}$, we find, through Eqs. (18), the following asymptotic behaviors:

$$\mu'\sim l^{d-1}\mu\ ,$$
$$K'\sim\mu'\ , \tag{32}$$
$$J'\sim f_1(d,J)\ ,$$

where $f_1(d,J)$ is given by Eq. (26). From Eqs. (32) we find, for $d=3$, four fixed points: $(\mu,K,J)=(-\infty,-\infty,J_c^A)$, $(-\infty,-\infty,J_2^A)$, $(-\infty,-\infty,J_c^F)$, and $(-\infty,-\infty,-\infty)$. In this limit $(\mu\to-\infty)$ the Jacobian of the recurrence equations (18) evaluated at any of the just-mentioned fixed points exhibits an eigenvalue $\lambda=l^d$, which is associated with the eigenvector $(\mu,K,J)=(1,0,0)$. The physical meaning of all these fixed points will be clarified in Secs. IV and V.

IV. THE $d=2$ PHASE DIAGRAM

First of all, we analyze the $J=t=0$ cross section of the phase diagram in the (μ,K,J,t) space; this cross section is invariant under RG. The flow diagram resulting from Eqs. (18)–(20) is depicted in Fig. 3. We find three nontrivial fixed points in this subspace: the doubly unstable fixed point a, the singly unstable fixed point b, and [from Eq. (30)] the singly unstable fixed point $(\mu,K,J,t)=(-\infty,-\infty,0,0)|_{K=\mu+(3/4)\ln2}$ already discussed in Sec. III; which we denote by F_0 this last fixed point.

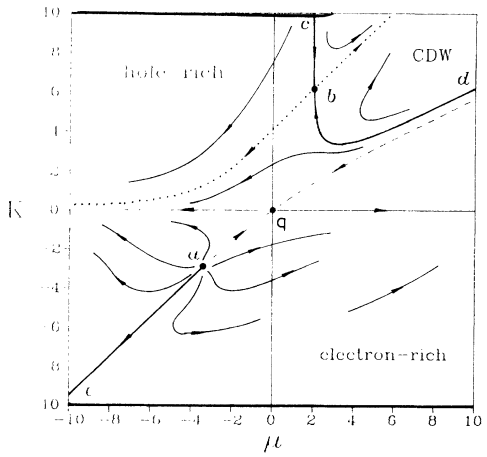

FIG. 3. Flow diagram in the invariant subspace (μ,K) for $d=2$. The RG flow is indicated schematically by arrows. The solid line *cbd* is a second-order transition line. The solid line *ea* corresponds to a first-order transition between the hole-rich and the electron-rich phases; this line ends at the critical point *a*; the dashed line corresponds to a smooth continuation between the two phases. The dotted line is associated with the relevant scaling field at the fixed point *b*.

All points belonging to the line *ea* of Fig. 3 are attracted by the fixed point F_0. The relevant eigenvalue of the recurrence equations linearized at this point equals $\lambda=l^d$ $(l=3)$ and corresponds to the eigendirection $(\mu,K)=(1,0)$. Since the chemical potential μ is the ordering field associated with the order parameter n, this result shows that the fixed point F_0 fulfills the Nienhuis and Nauenberg condition[19] for a first-order phase transition fixed point. In other words, the line *ea*, which has the $\mu\to-\infty$ asymptotic form indicated in Eq. (29), is a first-order transition line (two-phase coexistence) between the hole-rich and the electron-rich phases, respectively defined as the complete basins of attraction of the fully attractive fixed points h and p; this line ends at the critical point a. The basin of attraction of the fixed point q (dashed line in Fig. 3) corresponds to a smooth transformation of one phase into the other, i.e., the density of electrons n changes smoothly when passing through this line. The correlation length and the correlation function critical exponentials at the critical point a are given, respectively, by $\nu_a=\ln l/\ln\lambda_a^{(1)}$ and by $\eta_a=d+2(1-\ln l/\ln\lambda_a^{(2)})$, where $\lambda_a^{(1)}$ and $\lambda_a^{(2)}$ are the eigenvalues of the recurrence equations linearized at the fixed point a (the associated eigenvectors are, respectively, tangential and normal to the line *ea*).

All the points belonging to the region in the plane (μ,K) enclosed by the line *cbd* in Fig. 3 are attracted by the fully stable fixed point $(\mu,K,J,t)=(+\infty,+\infty,0,0)|_{K=\mu+\gamma}$, with $\gamma\approx4$; we denote this fixed point by w. This fixed point characterizes the CDW phase discussed in Sec. III. All points on the line *cbd* in Fig. 3 are attracted by the fixed point b. This line corresponds to a second-order (continuous) phase transition between the hole-rich and the CDW phases. The corresponding correlation length critical exponent is given by $\nu_b=\ln l/\ln\lambda_b$, where λ_b is the relevant eigenvalue at the point b (the associated eigenvector is tangential to the dotted line shown in Fig. 3). All the numerical values of the above-described fixed points and their general characteristics are summarized in Table I.

The fixed-point structure shown in the $J=t=0$ subspace completely determines the flow of points in the full parameter space (μ,K,J,t) for $d=2$ because all the points outside of this subspace are attracted into it, i.e., its flow is driven by the set of fixed points located at the $J=t=0$ subspace; the different transition hypersurfaces are governed by the above-described nontrivial fixed points. We now describe several representative projections of the $d=2$ complete phase diagram.

Let us now analyze the $t=0$ projection of the phase diagram for $J>0$ (the $J<0$ part of the phase diagram is completely analogous to the $J>0$ one). In Fig. 4, we show the $K<0$ (attractive charge interaction) and $\mu<0$ region of the phase diagram. There is a first-order transition surface between the hole-rich and the electron-rich phases. This surface is governed by the fixed point F_0 and extends the line *ea* shown in Fig. 3; this surface ends at a critical line (denoted by *af* in Fig. 3) whose points are governed by the fixed point a. The first-order surface,

TABLE I. Classification, locations, and critical exponents of the fixed points underlying the $d=2$ phsae diagram of the t-J model. All the fixed points in this table are located at the invariant subspace $(\mu,K,J,t)=(\mu,K,0,0)$; PE and PH, respectively, stand for the paramagnetic electron-rich and hole-rich phases; CDW stands for the charge-density-wave phase.

Fixed point	Location (μ,K)	Stability	Domain in (μ,K,J,t) space	Relevant eigenvalues
q	(0,0)	Singly unstable	Smooth continuation hypersurface between PH and PE phases	$\lambda=l^{d-1}=3$
p	$(+\infty,0)$	Fully stable	PE phase	
h	$(-\infty,0)$	Fully stable	PH phase	
w	$(\infty,\infty)\vert_{K=\mu+\gamma}$	Fully stable	CDW phase	
F_0	$(-\infty,-\infty)\vert_{K=\mu+\alpha_0}$	Singly unstable	First-order hypersurface between PE and PH phases	$\lambda=l^d=3$
a	$(-3.42,-2.93)$	Doubly unstable	Critical surface	$\lambda_a^{(1)}\approx 2.27$ $\lambda_a^{(2)}\approx 7.84$
b	(2.03,6.14)	Singly unstable	Critical hypersurface between PH and CDW phases	$\lambda_b\approx 2.80$

as well as the critical line, extends to the $K>0$ and $\mu<0$ region.

In Fig. 5, we show the $K>0$ (repulsive charge interaction) and $\mu>0$ region of the phase diagram. A second-order transition surface between the hole-rich and the CDW phases appears. This surface (which is an extension of the line *cbd* of Fig. 3) is governed by the fixed point b. The second-order surface separates the CDW phase from the hole-rich one.

The general structure of the $t\neq 0$ phase diagram repeats that of the $t=0$ one. The $K=0$ phase diagram [which is associated with the Hamiltonian (1)] is depicted in Fig. 6. For $\mu<0$, we find again a first-order transition surface between the hole-rich (below the surface) and the electron-rich (above the surface) phases. This surface ends at a critical line (denoted by *gh* in Fig. 6) governed by the fixed point a of Fig. 3. The critical value of J increases with t. No CDW phases exists for $K=0$.

The general structure of the full $d=2$ phase diagram in the (μ,K,J,t) can be summarized as follows.

(1) Three phases are present: hole rich, electron rich, and CDW.

(2) For $\mu<0$, there is a first-order transition hypersurface between the hole-rich and the electron-rich phases, which ends at a critical surface.

(3) For $\mu>0$ and $K>0$, there is a second-order transition hypersurface between the hole-rich and the CDW phases.

(4) For $\mu>0$, the transition between the hole-rich and the electron-rich phases is smooth (in the sense that there is a smooth change of the electron density).

A representative cross section of the phase diagram for typical K and t values is shown in Fig. 7. A complete list of the fixed points underlying the $d=2$ phase diagram and their general characteristics is presented in Table I.

The problem of phase separation (two-phase coexistence) in the $d=2$ t-J model at zero temperature has been previously treated by Emery *et al.*;[20] such work suggests that a phase separation occurs for *all* values of J/t. This is in variance with our results. Indeed, let us analyze the phase diagram in terms of the temperature-independent variables J/t, μ/t, and of the dimensionless temperature $1/t$. In Fig. 8, we show the coexistence lines in the $(\mu/t,1/t)$ plane for $K=0$ and constant J/t, for several values of J/t. Each line ends at a critical point whose corresponding critical temperature $(1/t)_c$ decreases with J/t. In Fig. 9, we show the critical temperature $(1/t)_c$ as a function of J/t. Numerical errors make it extremely difficult to get accurate results for very low temperatures $(1/t<0.1)$. However, our results suggest that a critical value $(J/t)_c$ exists below which the first-order transition disappears for all temperatures, i.e., *the system does not phase separate for low J/t.* From Fig. 9,

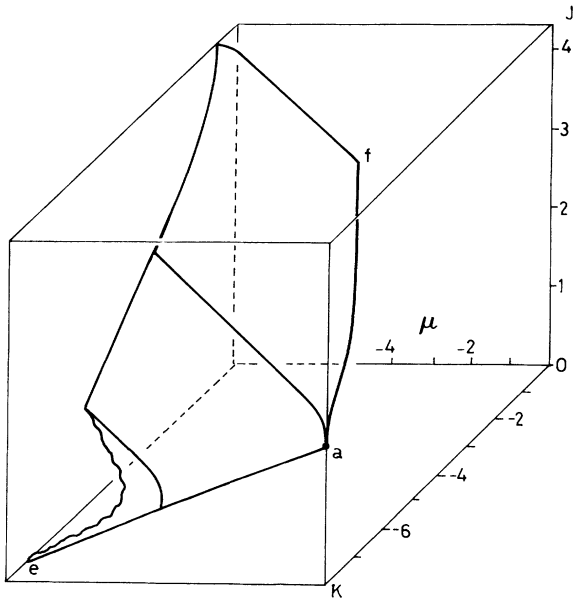

FIG. 4. Phase diagram for $t=0$ and $K<0$ in $d=2$. The surface *eaf* corresponds to a first-order transition between the hole-rich and the electron-rich phases. This surface ends at the critical line *af* and extends to the $\mu<0$, $K>0$ region.

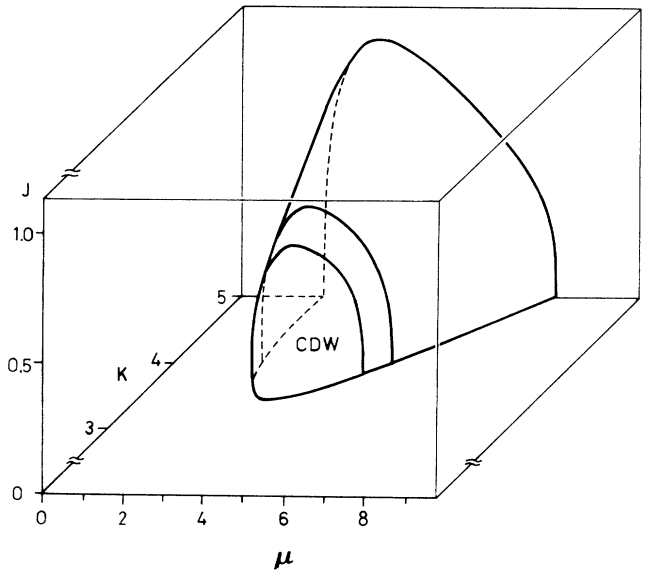

FIG. 5. Second-order transition surface between the hole-rich and the CDW phases for $t=0$ and $J>0$ in $d=2$.

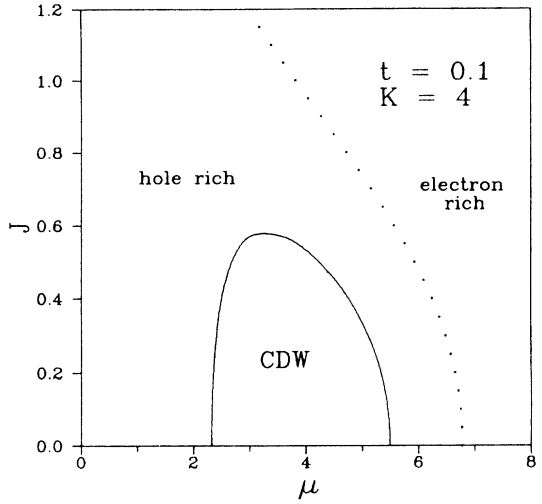

FIG. 7. Representative cross section of the $d=2$ phase diagram for typical values of the parameters t and K. The dotted line corresponds to a smooth continuation between the hole-rich and the electron-rich phases.

we extrapolate the value $(J/t)_c \approx 1.4$. It is interesting to repeat the above analysis for the case $K=-J$. The results we have obtained are analogous to those for the $K=0$ case. For $K=-J$, the extrapolated value of $(J/t)_c$ is $(J/t)_c \approx 0.67$. This result suggests that the Hubbard model does not show phase separation, at least for high values of U/t where similarities are expected between the t-J and Hubbard models. This conclusion is in agreement with recent Monte Carlo calculations on the Hubbard model.[21]

V. THE $d=3$ PHASE DIAGRAM

Now we present the phase diagram generated by the recurrence equation (16) for $d=3$. Although many of the features of the $d=2$ phase diagram persist for $d=3$, the phase diagram in this case is appreciably modified because the spin interactions related to continuous group symmetries give rise to long-range magnetic order. So, a very interesting and complex phase diagram appears. Since all the relevant fixed points, i.e., those which completely determine the critical properties of the model, are located at the $t=0$ subspace (invariant under RG); we start our discussion with this case.

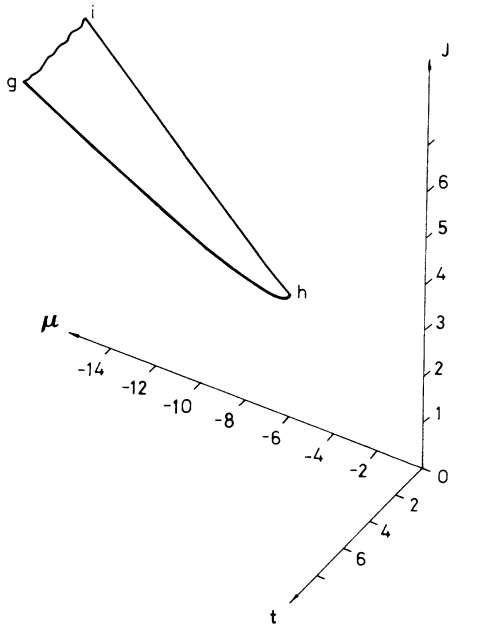

FIG. 6. Phase diagram of the $d=2$ t-J model ($K=0$). The picture shows a first-order transition surface from the hole-rich (small values of J) to the electron-rich (high values of J) phases. This surface ends at the critical line gh; the ih line lies on the $t=0$ plane. Another similar surface exists for $J<0$.

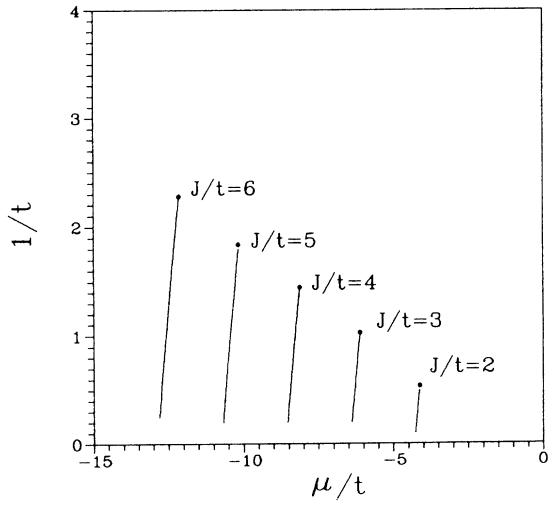

FIG. 8. Coexistence lines (first-order transitions) for $K=0$ and typical values of J/t in $d=2$. Each line ends at a critical point as the dimensionless temperature $1/t$ increases.

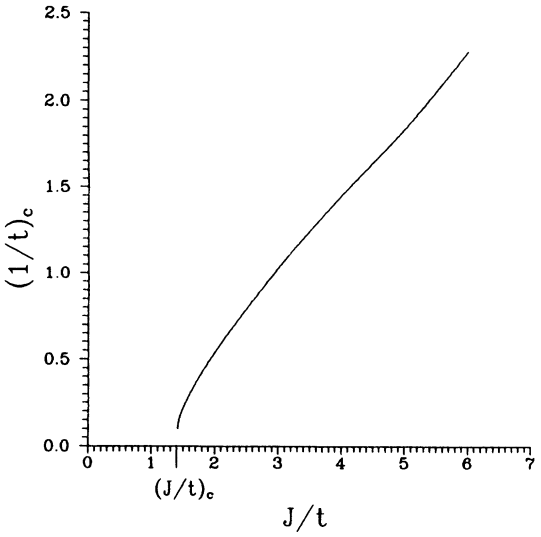

FIG. 9. Dimensionless critical temperature $(1/t_c)$ as a function of J/t for $K=0$ in $d=2$ (see Fig. 7). The curve suggests that $(1/t)_c \to 0$ for $J/t \to (J/t)_c$. The extrapolated value of $(J/t)_c$ is $(J/t)_c \approx 1.4$.

A. The $t=0$ phase diagram

As we said above, all the relevant fixed points lie in the $t=0$ subspace. In other words, all the points in the (μ,K,J,t) parameter space are driven to this subspace under the RG transformation.

We start our analysis with the $J=t=0$ invariant subspace. The general fixed-point structure in this subspace is qualitatively analogous to the fixed-point structure at $d=2$ (see Sec. IV and Fig. 3). The numerical values of the fixed points in this subspace and their general characteristics are presented in Table II, where the notation for the fixed points is the same as in $d=2$. All the eigenvalues of the linearized recurrence equations corresponding to the scaling fields associated with the t and J parameters at every fixed point are irrelevant, i.e., all fixed points are attractive in such directions. For $J=0$ there is no long-range magnetic order. In order to emphasize the paramagnetic nature of the hole-rich and electron-rich phases, we now denote them as PH *(paramagnetic hole rich)* and PE *(paramagnetic electron rich)*, respectively.

The phase diagram for $J>0$ and $K<0$ is shown in Fig. 10 and the set of fixed points for $J>0$ which determines its structure is shown in Table III. The global connectivity of all the fixed points for $J \geq 0$ is schematically depicted in Fig. 11. As expected, this phase diagram shows qualitatively a great similarity with the RG phase diagram of the classical $d=2$ BEG model (see Ref. 17). Three phases are present for $K<0$: (i) the PH phase below the *FMT* surface; (ii) the PE phase below the *FTC* surface, and (iii) an antiferromagnetically (AF) ordered phase located above the surface *FMTC*. These phases are defined, respectively, as the basins of attraction of the fixed points h, p, and $(\mu,K,J,)=(+\infty,K_2^A,J_2^A)$ hereafter denoted by A. The surface *FTC* is governed by the critical fixed point $(\mu,K,J)=(+\infty,K_c^A,J_c^A)$, which we denote as C_A. The fixed points A and C_A emerge from Eqs. (25)–(26). Consequently, this surface corresponds to a second-order transition between the PE and AF phases. The corresponding correlation length critical exponent is given by $\nu_A=\ln l/\ln\lambda_A$, where

$$\lambda_A=\left.\frac{\partial f_1(3,J)}{\partial_J}\right|_{J_c^A}.$$

The *FMT* surface is governed by the fixed point $(\mu,K,J)=(-\infty,-\infty,J_2^A)$, hereafter denoted by F_A. As we have seen in Sec. III, this fixed point is attractive in all directions but one, namely, that associated with the ordering field μ, whose corresponding eigenvalue is $\lambda=l^d$. Since the electron density in the AF phase satisfies $n\approx 1$ ($\mu=+\infty$ at the fixed point A), *FMT* is a first-order transition surface between the PH and the AF phases.

The surface *FEae* is governed by the fixed point F_0. The characteristics of this fixed point for $d=2$ were already discussed in Sec. IV. Through the same arguments we see that the *FEae* surface is a first-order transition one

TABLE II. Classification, locations, and critical exponents of the fixed points at the invariant subspace $J=t=0$ for $d=3$. The connectivity between the different fixed points is the same as in the $d=2$ case (see Fig. 3). See caption of Table I.

Fixed point	Location (μ,K)	Domain in (μ,K,J,t) space	Relevant eigenvalues
q	(0,0)	Smooth continuation boundary between PH and PE phases	$\lambda=l^{d-1}=9$
p	$(+\infty,0)$	PE phase	
h	$(-\infty,0)$	PH phase	
w	$(\infty,\infty)\vert_{K=\mu+\gamma}$ $\gamma\approx 12.48$	CDW phase	
F_0	$(-\infty,-\infty)\vert_{K=\mu+\alpha_0}$ $\alpha_0=\frac{9}{13}\ln 2$	First-order hypersurface between PE and PH phases	$\lambda=l^d=27$
a	$(-1.82,-1.47)$	Critical surface	$\lambda_a^{(1)}\approx 8.27$ $\lambda_a^{(2)}\approx 11.33$
b	(1.44,14.43)	Critical hypersurface between PH and CDW phases	$\lambda_b\approx 8.10$

TABLE III. Classification, locations, and relevant eigenvalues of the fixed points for $J>0$ and $t=0$, underlying the phase diagram shown in Fig. 10. These fixed points, together with those shown in Table II, completely determine the $d=3$ phase diagram for $J>0$; PH and PE, respectively, stand for paramagnetic hole-rich and electron-rich phases, AF stands for the antiferromagnetic phase.

Fixed point	Location (μ,K,J)	Stability	Domain in (μ,K,J,t) space	Relevant eigenvalues
A	$(+\infty,K_2^A,J_2^A)$	Fully stable	AF phase	
C_A	$(+\infty,K_c^A,J_c^A)$	Singly unstable	Second-order hypersurface between PE and AF phases	$\lambda_A\approx 2.42$
F_A	$(-\infty,-\infty,J_2^A)$	Singly unstable	First-order hypersurface between PH and AF phases	$\lambda=l^d=27$
G_A	$(-\infty,-\infty,J_c^A)$	Doubly unstable	Critical end-point surface	$\lambda_A,\lambda=l^d$
T	$(-1.02,-0.01,0.70)$	Doubly unstable	Tricritical surface	$\lambda_T^{(1)}\approx 12.87$ $\lambda_T^{(2)}\approx 1.57$
E	$(-1,72,-0.97,0.49)$	Triple unstable	Special multicritical line	$\lambda_E^{(1)}\approx 16.32$ $\lambda_E^{(2)}\approx 2.74$ $\lambda_E^{(3)}\approx 1.66$

between the PH and the PE phases. This surface ends at the isolated critical line aE, which is governed by the fixed point a.

The FMT and FTC surfaces join smoothly at the line FT. The fixed points E and T on this line are nontrivial ones. The fixed point T is attractive along the line ET, i.e., the eigenvalue whose eigenvector is tangential to the line ET satisfies $\lambda<1$. Also, the fixed point T has two relevant eigenvalues $(\lambda_T^{(1)}>\lambda_T^{(2)}>1)$, whose associated eigenvectors are, respectively, transversal and tangential to the transition surface. This structure is characteristic of tricritical behavior and therefore the ET line is a tricritical one.[22] The tricritical exponents are given by $\nu_t=\ln l/\ln\lambda_T^{(1)}$ and $\phi_t=\ln\lambda_T^{(2)}/\ln\lambda_T^{(1)}$. The numerical values of the different relevant eigenvalues are shown in Table III. The two first-order surfaces FMT and $FEae$, and the second-order surface FTC meet along the line FE, where the two first-order surfaces have equal slopes. The line FE is governed by the fixed point $(\mu,K,J)=(-\infty,-\infty,J_c^A)$, which we denote by G_A. As we have seen in Sec. III, this fixed point has two relevant eigenvalues: one first-order eigenvalue $\lambda=l^d$ coupled to the field μ and thus giving a first-order transition in the density n, and the other $\lambda=l^{1/\nu_A}$ giving the same critical behavior

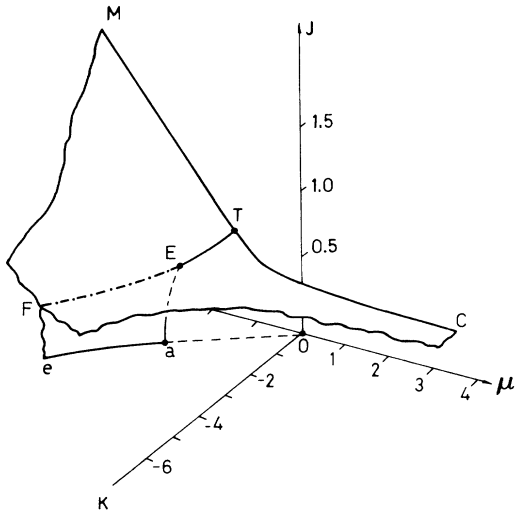

FIG. 10. Phase diagram for $t=0$ and $K<0$ in $d=3$. The region above the surface $FMTC$ corresponds to an antiferromagnetic (AF) phase; the region below the surface FTC corresponds to a paramagnetic electron-rich phase (PE) while the region below the surface FMT corresponds to a paramagnetic hole-rich phase (PH). The surface FTC is an AF-PE second-order transition surface, while the surface FMT is an AF-PH first-order one; the surface $eaEF$ is a PH-PE first-order one and it ends at the isolated critical line aE. The dash-dotted line FE is a critical-end line, while the solid line ET is a tricritical one.

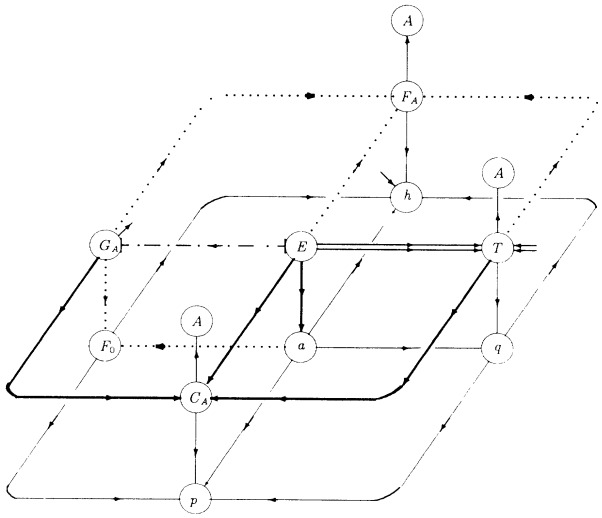

FIG. 11. Schematic diagram showing the global connectivity of the set of fixed points which determine the phase diagram of Fig. 10. The dark solid and dotted lines correspond to RG trajectories respectively flowing through second- and first-order surfaces; the double-dark solid and dash-dotted lines respectively correspond to the tricritical and critical-end lines; light trajectories do not correspond to any phase transition. The numerical values and the general characteristics of all the fixed points are listed in Tables II and III.

as the fixed point C_A. The fixed point G_A is unstable towards C_A (see Fig. 11) with $\lambda=l^d$ and unstable towards F_0 and F_A with $\lambda=l^{1/\nu_A}$. This structure is characteristic of critical end-point behavior and the *FE* line is made of critical end points *(critical end line)*. The tricritical line *ET*, the critical line *aE*, and the critical end line *FE* join at the fixed point *E*. This point has three relevant eigenvalues $(\lambda_E^{(1)}>\lambda_E^{(2)}>\lambda_E^{(2)}>1)$ thus being a multicritical point. The analogous point in the classical BEG model describes a special tricritical point associated with the three-state Potts model transition.[17,23] This fixed point is probably related to some quantum analog of the three-state model.

The transition surface between the antiferromagnetic and the paramagnetic phases (including both first- and second-order regions as well as the tricritical line) extends to the $K>0$ region of the parameter space. Below this surface there appears, for $\mu>0$, a second-order transition surface between the hole-rich and the CDW (enclosed by the second-order surface) phases; this surface is analogous to the one encountered in Sec. IV (see Fig. 5) and is governed by the fixed point *b*. In Fig. 12, we show some typical constant-K cross sections of the phase diagram for $J>0$.

The phase diagram for $t=0$ and $J<0$ shows the same qualitative structure as the above described $(J>0)$, the antiferromagnetic phase being now replaced by a ferromagnetic one. For each of the fixed points for $J>0$ there exists an analogous one for $J<0$; its locations and general characteristics are listed in Table IV. The global connectivity between the different fixed points is the same as that shown in Fig. 11 for the corresponding set for $J>0$.

B. The $t\neq 0$ phase diagram

As stated at the beginning of this section, all the points in the parameter space (μ,K,J,t) are governed by the fixed points located at the invariant subspace $t=0$. Then the first- and second-order surfaces become three-dimensional hypersurfaces in the complete parameter space, while the tricritical and critical-end lines become two-dimensional hypersurfaces. The special multicritical fixed points generate isolated multicritical lines which are

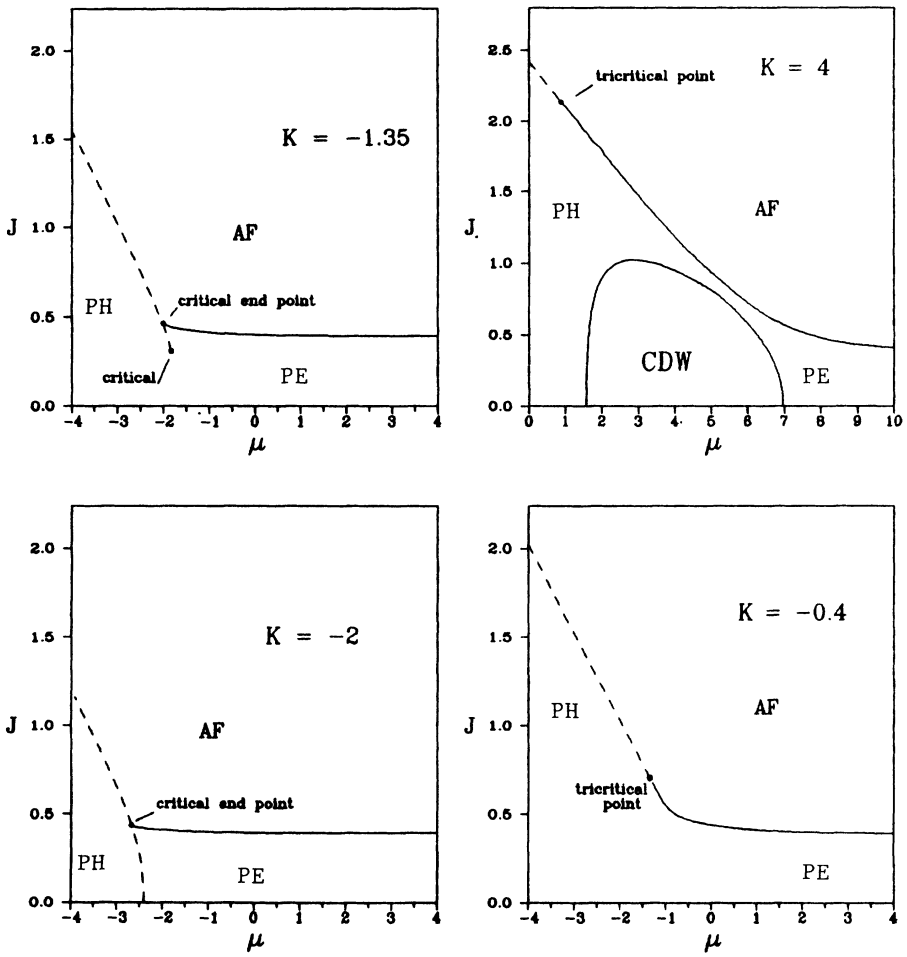

FIG. 12. Typical constant-K cross sections of the $d=3$ phase diagram for $t=0$. Dashed and solid lines, respectively, correspond to first- and secod-order phase transitions.

TABLE IV. Classification, locations, and critical exponents of the fixed points for $J<0$ and $t=0$. These fixed points, together with those shown in Table II, completely determine the $d=3$ phase diagram for $J<0$; F stands for the ferromagnetic phase. The general connectivity between the different fixed points is the same as that shown in Fig. 11 for the corresponding $J>0$ set of fixed points.

Fixed point	Location (μ,K,J)	Stability	Domain in (μ,K,J,t) space	Relevant eigenvalues
F_F	$(+\infty,+\infty,-\infty)$	Fully stable	F phase	
C_F	$(+\infty,K_c^F,J_c^F)$	Singly unstable	Second-order hypersurface between PE and F phases	$\lambda_F\approx 2.03$
F_F	$(-\infty,-\infty,-\infty)$	Singly unstable	First-order hypersurface between PH and F phases	$\lambda=l^d=27$
G_F	$(-\infty,-\infty,J_c^F)$	Doubly unstable	Critical end-point surface	$\lambda_F,\lambda=l^d$
T	$(-1.54,-0.36,-1.15)$	Doubly unstable	Tricritical surface	$\lambda_T^{(1)}\approx 15.41$ $\lambda_T^{(2)}\approx 2.18$
E	$(-1.76,-1.10,-0.58)$	Triple unstable	Special multicritical line	$\lambda_E^{(1)}\approx 16.87$ $\lambda_E^{(2)}\approx 2.96$ $\lambda_E^{(3)}\approx 1.38$

located at the boundary between the tricritical and critical-end surfaces. We now analyze some particular cases.

In Fig. 13, we show some typical constant-t cross sections of the phase diagram for $K=0$ and $J>0$. For $K=0$ the transition between the PH and PE phases is smooth everywhere but for a small first-order line for $t\gtrsim 3$; this line is located very close to the second-order line. For high values of t and low values of J, we observe the appearance of a ferromagnetic (F) phase, i.e., a region

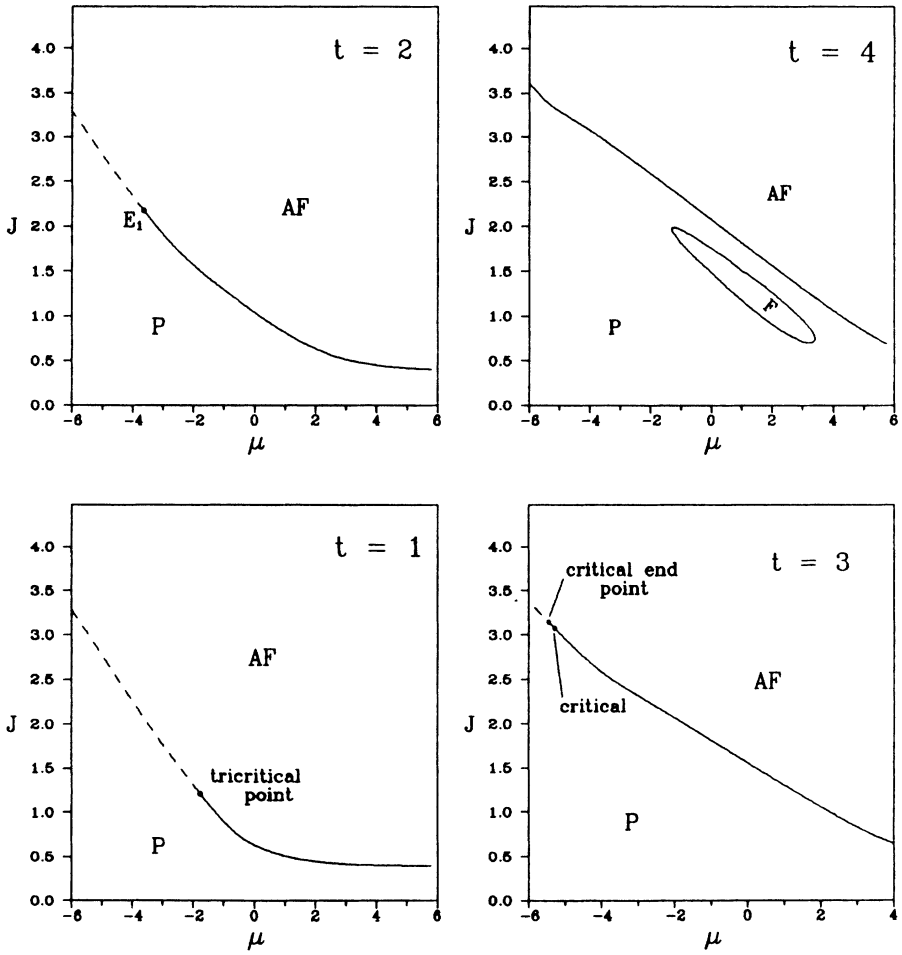

FIG. 13. Typical constant-t cross sections of the $d=3$ phase diagram for $K=0$. Dashed and solid lines, respectively, correspond to first- and second-order phase transitions. The point E_1 is a special multicritical one. For $t=3$, the first-order line between PH and PE and the second-order line are too closely located to be resolved in the present scales.

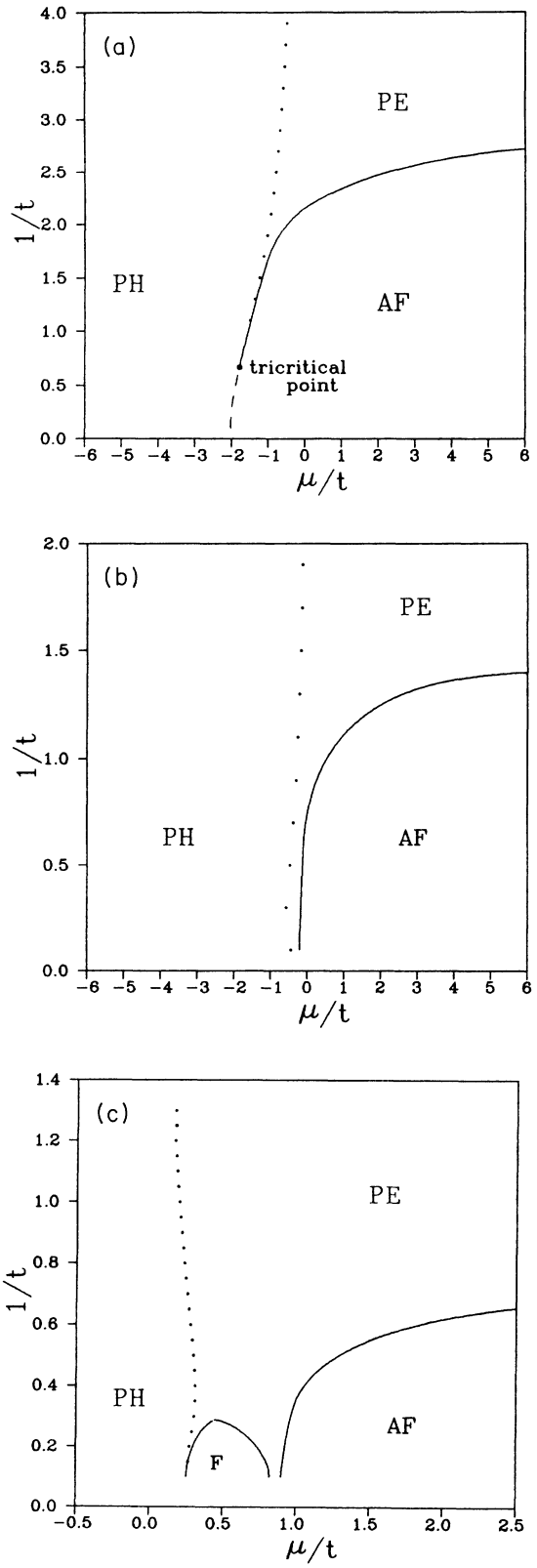

FIG. 14. Phase diagrams in the $(\mu/t, 1/t)$ space for $K=0$ and typical values of J/t. Dashed and solid lines, respectively, correspond to first- and second-order transitions; dotted lines correspond to a smooth change in the density n and do not describe any phase transition. (a) $J/t=1$; (b) $J/t=0.5$; (c) $J/t=0.25$.

of the parameter space governed by the fully stable fixed point F_F (see Table IV). This region is bounded by a second-order transition surface to the PE phase. The presence of an F phase can be better understood by analyzing the phase diagram in terms of the variables $(\mu/t, J/t, 1/t)$. Indeed, in Fig. 14, we show some typical constant-J/t phase diagrams for $K=0$ and different values of J/t. In Fig. 14(c), we see that the F phase appears at low temperatures $1/t$, for low values of the parameter J/t, precisely where the t-J model is expected to present a behavior similar to that of the Hubbard model for high values of U/t.[24] It is a known result[25,26] that a hole in a half-filled Hubbard model tends to form a ferromagnetically ordered region around itself, sometimes called a ferromagnetic polaron. On the basis of these results, and various approximate methods, such as Hartree-Fock,[27] it is believed that the Hubbard model has a ferromagnetic ground state for some range of hole concentrations. Moreover, many approaches predict a finite-temperature phase transition into ferromagnetic state.[28–30] Therefore, the F phase in the three-dimensional t-J model can be understood in terms of fer-

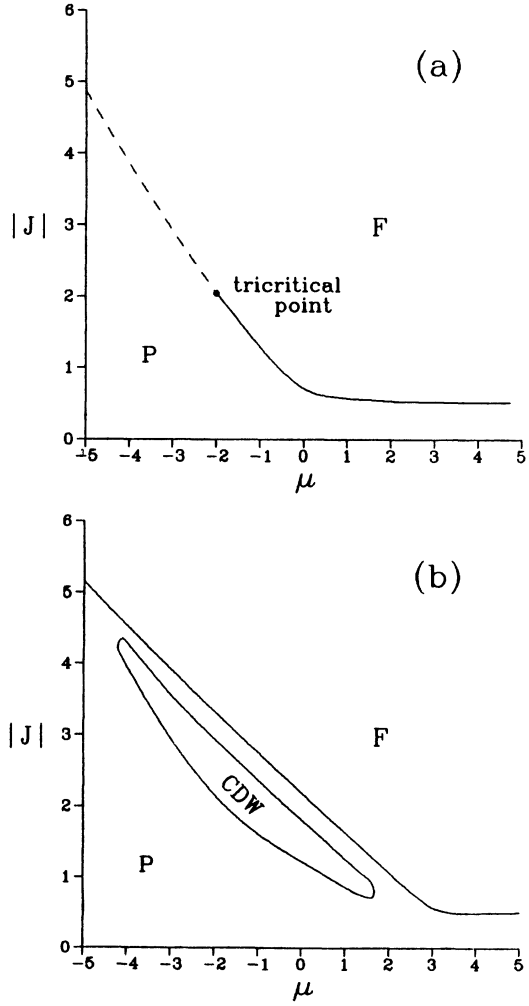

FIG. 15. Typical constant-t cross sections of the $d=3$ phase diagram for $J<0$ and $K=0$; P and F, respectively, stand for paramagnetic and ferrommagnetic. (a) $t=1$; (b) $t=3$.

romagnetic polarons. The F phase disappears when J/t is increased.

We observe that the system is antiferromagnetically ordered at low temperatures for all values of J/t and low concentration of holes (i.e., for high values of μ). The AF order is destroyed when the concentration of holes is increased, i.e., by lowering μ. Several experiments show that doping with holes destroys the Néel state in La and Y copper-oxide compounds.[4,5,31–33] For high values of J/t and low temperatures, this transition can be a first-order one (with a tricritical point separating the second- and first-order transition lines), i.e., we get, as in the two-dimensional case, phase separation, but now the electron-rich phase is antiferromagnetically ordered. Indeed, NQR (Ref. 32) and muon-spin resonance[33] in La compounds suggest that the magnetic transition could be a first-order one for some range of hole concentration. Moreover, the observed anomalies in the NQR relaxation rates could be indicative of tricritical behavior.

Finally, we consider briefly the phase diagram for $J<0$. In Fig. 15, we show two typical cross sections of the phase diagram for $K=0$ and constant t. For low values of t, the general structure of the phase diagram is very similar to that of the $J>0$ one, the AF phase now being replaced by the F one. However, for high values of t, this similarity breaks. We observe in Fig. 15(b) that, for low values of $|J|$, the magnetic interactions induce a second-order phase transition into the CDW phase (compare Fig. 15 with Fig. 13).

VI. CONCLUDING REMARKS

We have performed a real-space RG analysis of the full finite-temperature magnetic phase diagram of a $d=2$ and 3 generalized t-J model; this phase diagram exhibits a very rich structure. In addition to the general interest of such a rich phase diagram, our results suggest that the phase diagram of several high-T_c materials (e.g., La- and Y-based copper-oxide compounds), at least as far as the magnetic properties are concerned, could be explained by a three-dimensional t-J model. Of course, the present model is too simple to get a numerically accurate description of such materials, but many improvements could be implemented. For instance, we see from Fig. 14 that, for the undoped system (i.e., for $\mu\rightarrow\infty$), $1/t\sim 1$, which corresponds to a Néel temperature $T_N\sim 10^5$ K (assuming a bandwidth ~ 1 eV). This value is, of course, unacceptably high. However, the interplane exchange couplings are very weak.[34] It is, therefore, reasonable to expect that a three-dimensional t-J model with strongly anisotropic exchange couplings will highly reduce the Néel temperature (it is not unreasonable to think that an anisotropy of the order of 10^{-3} could reduce T_N to the order of 100 K).

Our $d=2$ results predict that the t-J model does not show phase separation for low vales of J/t. This result indicates that the Hubbard model does not phase separate at finite temperature, at least for high values of U/t and possibly for all values U/t, a fact which is in agreement with recent Monte Carlo calculations. An interesting possibility would be to perform the present RG analysis of the Hubbard model for arbitrary values of U/t, both for $d=2$ and 3. This work is in progress and will be published elsewhere.

ACKNOWLEDGMENTS

Fruitful discussions with P. Serra are acknowledged. This work was partially supported by Grant Nos. PID 641/90 and 1707/90 from Consejo Provincial de Investigaciones Científicas y Technológicas de Córdoba (Argentina).

*e-mail: cannas@famaf.edu.ar.

[1]P. W. Anderson, Science **235**, 1196 (1987).
[2]K. A. Chao, J. S. Spalek, and A. M. Olés, J. Phys. C **10**, L271 (1977).
[3]F. C. Zhang and T. M. Rice, Phys. Rev. B **37**, 3759 (1988).
[4]D. Vaknin *et al.*, Phys. Rev. Lett. **58**, 2802 (1987).
[5]Y. Tranquada *et al.*, Phys. Rev. Lett. **60**, 156 (1988).
[6]S. Sarkar, J. Phys. A **23**, L409 (1990); P. A. Bares and G. Blatter, Phys. Rev. Lett. **64**, 2567 (1990).
[7]E. Dagotto, Int. J. Mod. Phys. B **5**, 907 (1991).
[8]K. H. Luk and D. L. Cox, Phys. Rev. B **41**, 4456 (1990).
[9]S. A. Cannas, F. A. Tamarit, and C. Tsallis, Solid State Commun. **78**, 685 (1991).
[10]J. D. Jorgensen *et al.*, Phys. Rev. B **38**, 11 337 (1988).
[11]P. Schlottmann, Phys. Rev. B **36**, 5177 (1987).
[12]Actually, in the strong-coupling expansion of the Hubbard model, other hopping terms appear which normally are not taken into account because they involve effective second-order long-range hoppings; also these terms are systematically eliminated in the present RG procedure.
[13]The charge term currently appears in the literature as $\frac{1}{4}n_i n_j$. The $\frac{1}{4}$ factor does not appear in expression (3) due to definition (2) of the spin operators, where we have eliminated the $\frac{1}{2}$ factor for simplicity.
[14]S. A. Cannas, F. A. Tamarit, and C. Tsallis, Phys. Rev. B **45**, 10 496 (1992).
[15]E. H. Lieb and F. Y. Wu, Phys. Rev. Lett. **20**, 1445 (1968).
[16]B. Blume, V. J. Emery, and R. B. Griffiths, Phys. Rev. A **4**, 1071 (1971).
[17]A. N. Berker and M. Wortis, Phys. Rev. B **14**, 4946 (1976).
[18]R. B. Griffiths, Physica **33**, 689 (1967).
[19]B. Nienhuis and M. Nauenberg, Phys. Rev. Lett. **35**, 477 (1975).
[20]V. J. Emery, S. A. Kivelson, and H. Q. Lin, Phys. Rev. Lett. **64**, 475 (1990).
[21]A. Moreo, D. Scalapino, and E. Dagotto, Phys. Rev. B **43**, 11 442 (1991).
[22]P. Pfeuty and G. Toulouse, *Introduction to the Renormalization Group and to Critical Phenomenas* (Wiley, New York, 1977).
[23]M. Kaufman *et al.*, Phys. Rev. B **23**, 3448 (1981).
[24]Although the map between the two models corresponds to $K=-J$, this case presents only minor modifications in the phase diagram corresponding to Fig. 14.

[25]Y. Nagaoka, Phys. Rev. **147**, 392 (1966).
[26]H. Takasaki, Phys. Rev. B **40**, 9192 (1989).
[27]D. Penn, Phys. Rev. **142**, 350 (1966).
[28]K. Kubo, Prog. Theor. Phys. **11**, 159 (1974).
[29]Bao-Hua Zhao *et al.*, Phys. Rev. B **36**, 2321 (1987).
[30]W. Nolting and W. Borgiel, Phys. Rev. B **39**, 6962 (1989).
[31]D. C. Johnston *et al.*, Phys. Rev. B **36**, 4007 (1987).
[32]K. Kumagai et al., Physica B **148**, 480 (1987).
[33]D. W. Harshman *et al.*, Phys. Rev. B **38**, 852 (1988).
[34]T. Thio *et al.*, Phys. Rev. B **38**, 905 (1988).